Korean J. Chem. Eng., 34(1), 54-61 (2017)
DOI: 10.1007/s11814-016-0237-9

pISSN: 0256-1115
eISSN: 1975-7220

Pneumatic transport characteristics of coarse size pulverized coal for the application of fast circulating fluidized bed gasification

Jin Wook Lee*,†, Seok Woo Chung*, Sang Oh Ryu*, Ji Eun Lee*, Yongseung Yun*, Chan Lee, Yongjeon Kim***, and Sungkwang Lim*****

*Plant Engineering Center, Institute for Advanced Engineering, Yongin 17180, Korea
**Department of Mechanical Engineering, Suwon University, Suwon 18323, Korea
***SK Innovation Global Technology, Daejeon 34124, Korea
(*Received 24 April 2016 • accepted 19 August 2016*)

Abstract−The pneumatic transport characteristics of pulverized coal with very coarse grain size were investigated, especially related to fast circulating fluidized bed gasifier. The lock hopper system was used along with the top discharge blow tank technology to examine the transportation characteristics of pulverized coal. The most important factors among the pulverized coal transportation properties were mass flow rate of pulverized coal and the solid loading ratio, which changed with the amount of fluidization nitrogen and differential pressure between injection hopper and gasifier. The mass flow rate of the pulverized coal and the solid loading ratio were linearly proportional to changes in differential pressure, and were inversely proportional to changes in the amount of fluidization nitrogen. In the case of extended transport line, similar feeding characteristics were obtained by increasing the differential pressure while the level of fluidization nitrogen was kept constant. Pressure losses were observed with changes in the mass flow rate of pulverized coal, solid loading ratio, and the transport gas density in horizontal and vertical, both upward and downward, straight pipelines and at bends. Characteristics of pressure losses under various operating conditions were correlated with the nondimensional numbers such as the Reynolds number, Froude number, solid/gas density ratio, and solid loading ratio. Such correlations were reasonably consistent with the experimental results.

Keywords: Pneumatic Transport, Large Size Pulverized Coal, Fast Circulating Fluidized Bed Gasification, Froude Number, Solid Loading Ratio

INTRODUCTION

Issues of global warming have boosted the proposition of significant reduction of greenhouse gas recently, and a consensus on reduction of fossil fuels consumption and new and renewable energy technologies has been established. However, the prospect for consumption rate of fossil fuels remains for decades to come and the fossil fuels should be consumed in cleaner way. More specifically, the various coal utilization technologies discharge the largest amount of carbon dioxide to produce the unit amount of energy. Therefore, the coal gasification technologies, especially the entrained bed gasification technologies and the related pilot plants, have been developed and operated by several advanced companies [1-5] and domestic research institutes [6,7], respectively, as a next generation clean coal technology. In view of the price volatility of high rank coal as a consequence of high oil prices fluctuation, the low rank coal utilization technology is also important. The system efficiency of entrained bed gasifier would decrease significantly at high temperatures over 1,400 °C-1,500 °C with the application of low rank coal due to the increased portion of sensible heat compared with the similar operation using the high rank coal. The fluidized bed gasification technology is an alternative technology to solve this problem via operation under the temperature of 1,000 °C [8]. The weakness of fluidized bed gasification technology is the low carbon conversion rate due to the low temperature operation. However, low rank coal has high reactivity to compensate for such a problem, and the recently developed technology utilizing the low rank coal with fast circulating fluidized bed gasification has been available [8]. The exact proportion of pulverized coal and oxidants should always be supplied for stable operation of the gasifier. The fast circulating fluidized bed gasification technology employs pulverized coal with higher moisture content and larger particles compared with those conventional pulverized coal combustion or entrained bed gasification technologies. In view of this, the pulverized coal with designated properties has to be supplied to the gasifier via a new technology.

Very tiny solid particles comprising the pulverized coal are transported downstream by the pneumatic transportation technology to storages or reactors. Such pneumatic transportation technology for tiny particles of the pulverized coal for combustion or gasification has also been widely used in chemical plants, steel mills, and cement or food industries [9-13]. The screw feeder or rotary valves are typically used for the transportation to the equipment operating under low pressure conditions. In this case, it is advantageous to control the pulverized coal feed and transport gas flow rates separately, although the leakage due to the rotating parts of the high

†To whom correspondence should be addressed.
E-mail: jwlee@iae.re.kr

pressure equipment might occur to some extent and the ensuing failures could also cause problems. Therefore, the lock hopper system comprised of successive pressure vessels without rotating parts is frequently used for high pressure operation [14].

In the present study, a pneumatic transport system for pulverized coal with very coarse particle sizes for the fast circulating fluidized bed gasification was intended to be observed. Since the fast circulating fluidized bed gasifier is to be operated at high pressure, the technology embodied in the lock hopper system was also applicable to feed the pulverized coal. The lock hopper feeding system continuously supplied the pulverized coal via the blow tank technology where the proper amount of fluidization gas is supplied inside of the injection hopper to fluidize and then discharge the pulverized coal through the pipeline installed inside the vessel [14]. More specifically, the essence of the present feeding technology comprised of the top discharge pressure vessel is connected to the fast circulating fluidized bed gasifier to examine the transportation characteristics of the pulverized coal to be supplied into the gasifier. Besides, the most important factors among pulverized coal transport characteristics turned out to be the mass flow rate of the pulverized coal and the solid loading ratio (the mass flow rate ratio of coal/N_2) as regulated via fluidization nitrogen and differential pressure between the injection hopper and gasifier.

The pressure loss characteristics in the transport line were estimated to be quite different from the ordinary pulverized coal combustor or entrained bed gasifier, owing to the significant differences in the physical properties of the loaded pulverized coal types. Therefore, the pressure loss characteristics observed in the horizontal and vertical (both upward and downward) pipelines and at the bends are attributed to the mass flow rate variation of the pulverized coal, solid loading ratio, and the transport gas density as affected by the operation pressure. The pressure loss characteristics under diverse operating conditions were correlated with the non-dimensional numbers such as Reynolds number, Froude number, solid/gas density ratio, and solid loading ratio.

PNEUMATIC TRANSPORT CHARACTERISTICS

Configuration of the pneumatic transportation equipment of the present study is illustrated in Fig. 1. The pulverized coal was stored in the lock hopper under normal pressure, and then in the injection hopper, where predetermined level of the pulverized coal was maintained via pressurization of the lock hopper to refill the into the injection hopper. The receiver tank was employed as a substitute for the gasifier, and for the continuous operation, the system was configured for recirculation from the receiver tank to the lock hopper. The nitrogen supply to the injection hopper for pressurization and fluidization was regulated using MFCs (mass flow controllers) and the set differential pressure between the injection hopper and the receiver tank was consistently maintained by partial discharge of the nitrogen through the pressure control valve installed at the injection hopper. Partial venting of nitrogen from the injection hopper was thus more efficient to consistently maintain the set differential pressure.

Table 1. Results of the proximate analysis and density analysis of Russian subbituminous coal

Analysis items		Value
Total moisture, wt%		9.53
Proximate analysis, air dry basis, wt%	Inherent moisture	8.66
	Volatile matter	41.74
	Fixed carbon	38.06
	Ash	11.54
Density, kg/m^3	Pure density	1,411
	Bulk density	810

A comprehensive proximate and density analyses results for the Russian subbituminous coal used in this study are summarized in Table 1. Initial moisture content of the pulverized coal was averaged to be about 9.5% after pulverization and partial drying, which was higher than the standard of the dry feeding entrained bed gasifier.

Particle size distribution of the pulverized Russian subbituminous coal is detailed in Fig. 2 and Table 2. The mean diameter of pulverized coal used for the fast circulating fluidized bed gasification was about 457 μm, which was again larger than those of ordinary entrained bed gasification or pulverized coal combustion.

Most importantly, effects of operation parameters on the pneumatic transportation of pulverized coal of larger particle sizes, as illustrated in Fig. 2 and Table 2, were investigated. Previous study [15] revealed that the top discharge pneumatic transportation of pulverized coal of 370 μm mean particle diameter was possible. For this, the differential pressure between the injection hopper and the gasifier and the amount of fluidization nitrogen were the most significant operational parameters governing the mass flow rate of the pulverized coal and the solid loading ratio. Therefore, in this study, the pneumatic transport characteristics of the pulverized coal

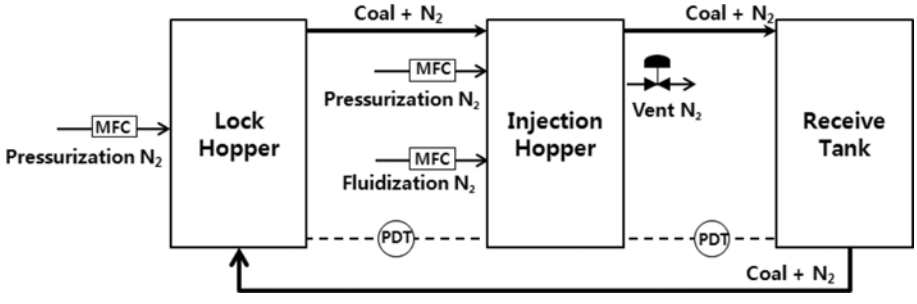

Fig. 1. Configuration of pneumatic transport system.

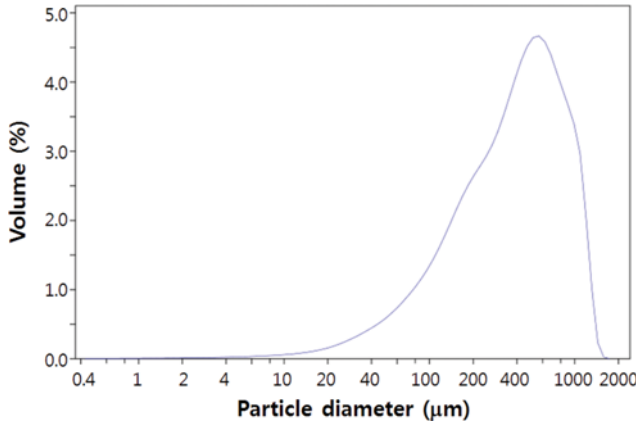

Fig. 2. Particle size distribution of pulverized coal used in this study.

having larger particle sizes was observed first, and then the pressure loss characteristics in transport lines were investigated. The 1/2 inch tube (inner diameter=10.93 mm) was employed as a transport line in all the experiments, and for the first experiment, the length of transport line was set to be 18 m with four bends in right angle to observe the pneumatic transport characteristics of pulverized coal along with the changes in differential pressure and the amount of fluidization nitrogen. For the next batch of experiments, the transport line extended to 36 m to observe the changes in pneumatic transport characteristics of pulverized coal.

To investigate the effects of differential pressure and the fluidization nitrogen flow on the pneumatic transport characteristics of the pulverized coal, the supply of pressurizing nitrogen for the injection hopper and the pressure of receiver tank were fixed at 35 Nm^3/h and 7.8 bar, respectively. Differential pressure and the fluidization nitrogen supply were initially fixed and then, after three minutes, the mass flow rate of the pulverized coal was measured by reading the weight difference of load cell every minute for over 10 minutes until the mass flow rate of the pulverized coal was stabilized, when the average values during the 10 minute interval was taken. And then again, the experiments of pneumatic transportation of pulverized coal were continued by changing the feed amount of fluidization nitrogen or by changing the differential pressure.

After completing the consecutive experiments mentioned above, results of changes in mass flow rate of pulverized coal and solid loading ratio according to changes in the most important factors in pneumatic transportation, the differential pressure between injection hopper and gasifier (in this study, it was the receive tank instead of the gasifier) and the feed amount of fluidization nitrogen, were obtained to find the quantitative and qualitative characteristics of pulverized coal transportation, and they are illustrated in Figs. 3 and 4, respectively. Above all, the trend of increase in mass flow rate of pulverized coal and solid loading ratio along with

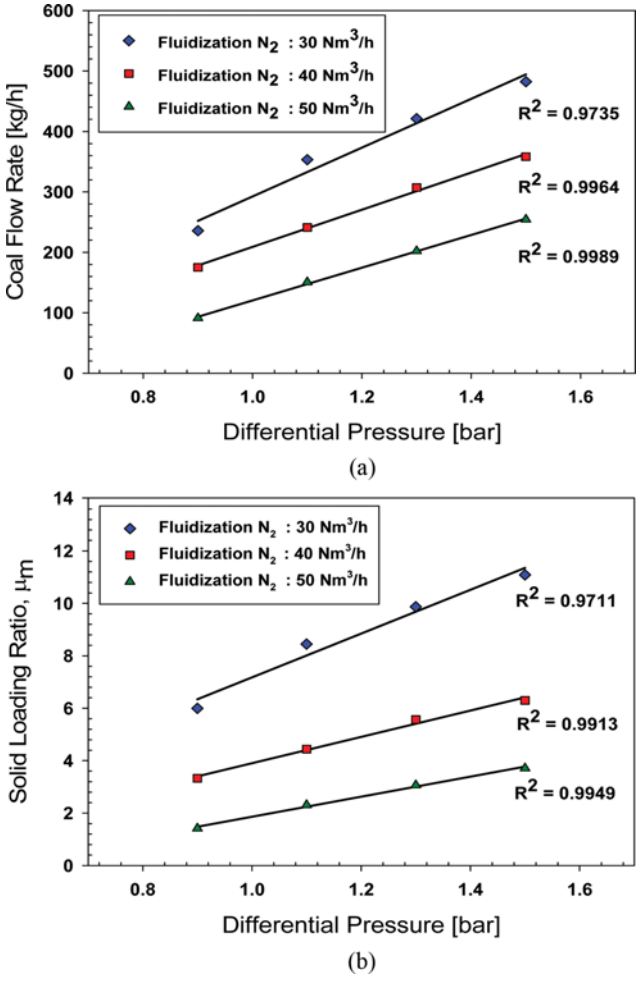

Fig. 3. (a) Changes in the mass flow rate of pulverized coal, and (b) changes in the solid loading ratio according to changes in the differential pressure and the amount of fluidization nitrogen (line length=18 m).

the increase of differential pressure, and the trend of overall decrease along with the increase in the amount of fluidization nitrogen are illustrated well. In Fig. 3, the changes in mass flow rate of pulverized coal and solid loading ratio varied according to changes in differential pressure in the case of 18 m of total length of transportation line were illustrated along with changes in the amount of fluidization nitrogen. The mass flow rate of the pulverized coal and the solid loading ratio linearly increased with the differential pressure, and decreased with the flow rate of the fluidization nitrogen under the equal level of differential pressure. The transport characteristics for 36 m total length of transport line are shown in Fig. 4 under equal operation pressure of 7.8 bar in the receiver tank. The differential pressure increased by about 0.4 bar with the

Table 2. Particle size distribution of pulverized coal used in this study

Particle size distribution (μm)					
Diameter at <10%	Diameter at <25%	Diameter at <50%	Diameter at <75%	Diameter at <90%	Mean
89.72	191.4	395.9	663.9	940.5	457.3

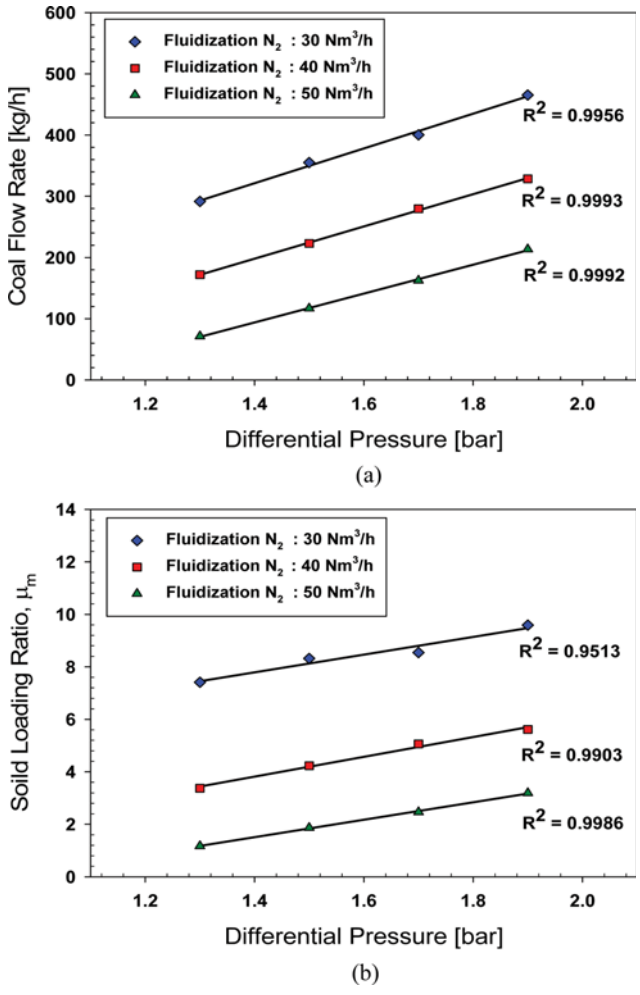

Fig. 4. (a) Changes in the mass flow rate of pulverized coal, and (b) changes in the solid loading ratio according to changes in the differential pressure and the amount of fluidization nitrogen (line length=36 m).

length of the transport line, which was attributed to the increased driving force caused by the higher pressure gradient compared with the 18 m total length of the transport line. However, the same flow rate of fluidization nitrogen was maintained at 30, 40, and 50 Nm^3/h as that in the case of 18 m transport line. Figs. 3 and 4 depict the ensuing variation of the differential pressure for increase of the transport line from 18 m to 36 m, where the similar trends of all the dependent variables are illustrated for the mass flow rate of the pulverized coal, the solid loading ratio, and the velocity and void fraction in the transport line. From these results, the similarity in all transport characteristics except requiring additional differential pressure corresponded to increased pressure loss due to extended length of horizontal transport line was identified. Thus it could be applicable to design changes or scale-up design requiring similar transport characteristics.

The variation of the transport velocity with the differential pressure and flow rate of the fluidization nitrogen remained in the range of 8-20 m/sec, and the void fraction (volume fraction of gas) of the mixture of pulverized coal and the fluidization nitrogen exceeded 90%. Considering these velocity levels exceeding the saltation velocity of 4-7 m/sec corresponding to the mass flow rate of the pulverized coal with the mean particle size of 450 μm and the solid loading ratio of this study and the resulting 90% void fraction of the mixture, it was estimated that the pulverized coal was transported in the continuous suspension flow regime. It was reported that the velocity over 1.5 times of the saltation velocity would be preferable to secure the stable continuous suspension flow [16]. Since it was calculated to be roughly 1.5 times of the saltation velocity for the flow rate of the fluidization nitrogen of 30 Nm^3/h, it was strongly inferred that the flow rate of the fluidization nitrogen should not be reduced further. If the flow rate of the fluidization nitrogen fell below this level or the differential pressure significantly dropped by the increased flow of the vented nitrogen to maintain the low differential pressure, the pulverized coal transportation could be. The saltation velocity was calculated using the following formula by Rizk [16,17].

$$v_{salt}=[4M_{solid}10^{a}g^{b/2}D^{(b/2-2)}/\rho_g\pi]^{1/(b+1)} \quad (1)$$

The M_{solid}, g, D, and ρ_g in the above expression denote the mass flow rate of the pulverized coal, gravitational acceleration, diameter of the transport pipeline, and the transport gas density, respectively. The a and b in the above expression were described in terms of the pulverized coal diameter, d_p,

$$a=1400d_p+1.96,\ b=1100d_p+250 \quad (2)$$

PRESSURE LOSS CHARACTERISTICS IN TRANSPORT LINES

In view of the results discussed above, the mass flow rate of pulverized coal, solid loading ratio, and other general characteristics were similar except the increase in differential pressure when the horizontal length of transport line was extended. To quantitatively describe variation of the differential pressure with operating pressure changes caused by scale-up design etc., non-dimensional numbers were used. At first, the pressure loss for the given length of horizontal or vertical pipelines or at bend should be expressed as in the following expressions of (3) and (4), where the friction coefficient f and the pressure loss coefficient K are appropriate non-dimensional numbers for particle suspension flow.

$$\text{straight line: } \Delta P=f\frac{L}{D}\frac{1}{2}\rho_g v_g^2 \quad (3)$$

$$\text{bend: } \Delta P=K\frac{1}{2}\rho_g v_g^2 \quad (4)$$

The gas velocity, v_g, is calculated by neglecting solid volume: $v_g=Q/A$, where Q and A denote volume flow rate of gas and cross sectional area of transport tube, respectively.

To derive Eqs. (3) and (4), the pressure loss for the actual operating conditions is to be obtained. For this, the transport line of Fig. 5 was additionally configured to the pneumatic transport system of Fig. 1 with differential pressure transmitters placed at each point. The same pulverized coal of Fig. 2 was used along with the same tube with 10.93 mm ID used in the previous experiment. The pressure loss for each condition was measured by changing the dif-

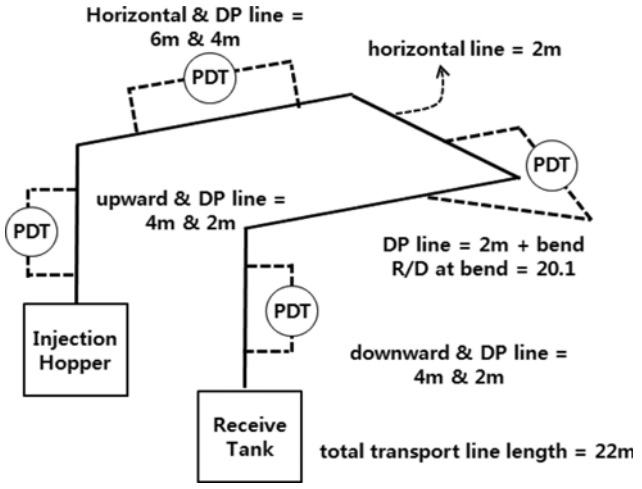

Fig. 5. The transport line configured for the experiment to measure pressure loss at each point.

ferential pressure between injection hopper and receive tank while the fluidization nitrogen was supplied under operation pressure of 7.8 bar. And then, the fluidization nitrogen pressure was increased to 12.3 bar to measure the corresponding pressure loss in the same way.

For measurement of the pressure losses at horizontal and vertical (both upward and downward) parts of the transport line and at bend, the equipment was configured to keep the spacing between starting and ending points of pressure loss 90 times of the tube diameter to secure the fully developed flow area. The transport line was also configured to keep the R/D ratio of the transport line diameter (D) and radius of curvature of the tube (R) to be about 20 at four bends points. In each experiment, fluidization nitrogen was appropriately pressurized to maintain the pressure in the injection hopper at suitable level and then the differential pressure between receive tank and injection hopper was adjusted to transport the pulverized coal. The mass flow rate of the pulverized coal and the reading from the four differential pressure transmitters at each condition were subsequently measured every minute to reach the quasi-steady state, when the mass flow rate readings were constant for more than 5 minutes. Due to the characteristic of gas-solid two phase flow, there can exist some range of fluctuation in the indicated values of differential pressure transmitter; thus the average value for 5 minutes' measurements was taken, and then the amount of fluidization nitrogen at each differential pressure was varied into five values to conduct the experiment. And the differential pressure was further increased to conduct the same experiments five times to measure the pressure losses at each point. After completion of the total 40 such experiments, results were assessed for validity: 39 experiments except the one which was considered to be insignificant due to its very small amount of pulverized coal transportation were accepted for derivation of the friction coefficients in straight line and the pressure loss coefficient at the bend via incorporation of the measured pressure loss into the Eqs. (3) and (4).

First, variation of the friction coefficient with transport velocity and the corresponding functional relationship was illustrated in Fig. 6 to fit the pressure loss characteristics into the straight line.

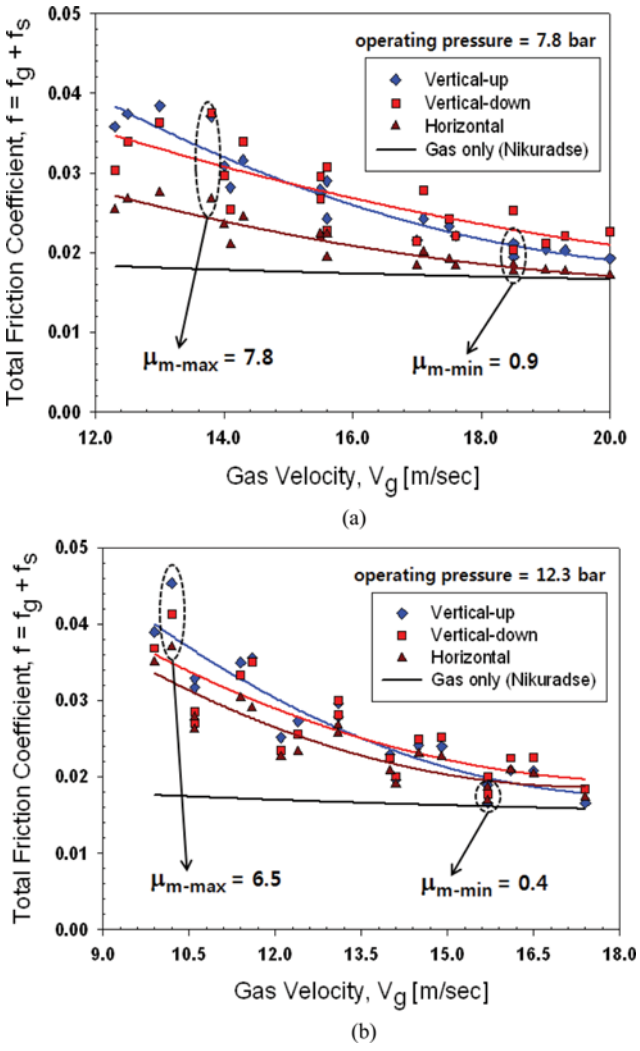

Fig. 6. Changes in friction coefficient of horizontal and vertical transport line along with varied transport velocity. Operation pressure of receiver tank=(a) 7.8 bar, and (b) 12.3 bar.

As the gravitational influence would be presumable, the friction coefficients in vertical direction appeared to be bigger than those of horizontal direction; and in the areas of low solid loading ratio, almost all the friction coefficients tended to converge in cases of pure gas flow. For vertical directions, the upward friction coefficient appeared to be larger than downward friction coefficients for low transport velocity and high solid loading ratio, while the reverse trend was observed for low solid loading ratio. The larger friction coefficient for upward flow seemed to be justified by some portion of the up-ward flowing particles for low transport gas velocity and high solid loading ratio, thus increasing the local number density caused by the gravity. However, the reverse trend for the high transport gas velocity and low solid loading ratio should be examined in further study. Though they were not introduced in this paper, results obtained from the numerical analyses conducted by authors of this paper showed the tendency of down-flowing particles to be concentrated toward the center of the pipeline in the area of low solid loading ratio compared to the up-flowing ones that might cause the local increase in particle number den-

sity, which could also increase the drag force [18,19]. Or there might be some measurement error in this low solid friction region where gravity effect is small. To clarify these results, further investigations should be carried out.

The friction coefficient illustrated in Fig. 6 is the integrated one resulting from the combined effects of transport gas and suspended solid particles which can be expressed as functions of 4 non-dimensional numbers: Reynolds number Re, Froude number Fr, solid-gas density ratio (ρ_s/ρ_g), and solid loading ratio μ_m. (M_{solid}/N_{gas}= mass flow rate ratio of coal to transport gas). Reynolds and Froude numbers are defined as follows:

$$\text{Reynolds number, } \mathrm{Re}=\frac{\rho_g v_g D}{\mu_g} \tag{5}$$

$$\text{Froude number, } \mathrm{Fr}=\frac{v_g}{\sqrt{(gD)}} \tag{6}$$

where each parameters are similarly defined to those in (1)-(4), as well as the μ_g, viscosity of transport gas.

And in general, the integrated friction coefficient f for flows with suspended solid particles can be expressed as a summation of the friction coefficient f_g for pure gas flow plus the influence of solid particles f_s as shown in the following expression (7) [20]:

$$f=f_g+f_s=f(\mathrm{Re})+f\left(\mathrm{Fr},\frac{\rho_s}{\rho_g},\mu_m\right) \tag{7}$$

For the cases of gas flow, the gravitational effect can be ignored for the friction coefficient inside the pipeline and the same functional expression can be commonly applied to both horizontal and vertical transport lines, and similar classical functional expressions have already been presented by several researchers: For example, Nikuradse's formula expressed f_g as a function of Re, as explained in the following expression (8) [20]. And for the friction coefficient f_s which integrated the combined effects of suspended solid particles, it can be further refined from (7) into an exponential function of Fr, ρ_s/ρ_g and μ_m as described by (9) [19].

$$f_g=f(\mathrm{Re})=0.0032+0.221/\mathrm{Re}^{0.237} \tag{8}$$

$$f_s=A\mathrm{Fr}^{\alpha}\left(\frac{\rho_s}{\rho_g}\right)^{\beta}\mu_m^{\gamma} \tag{9}$$

According to characteristics of particle sizes and moisture contents the constant values of A, α, β, and γ appearing in the expression (9) could generate diverse relational expressions. Prior studies identified the linear relationship between solid friction coefficient and solid loading ratio, and results of this study also showed a very linear relationship, even though not illustrated here; thus the exponent for the solid loading ratio γ was fixed by 1. Then the exponents for Froude number and density ratio that could maximize

Table 3. Exponents of non-dimensional parameters for solid friction coefficients in the transport line

	A	α	β	γ
Horizontal	132.6	−0.901	−1.691	1
Vertical, downward	0.108	−0.118	−0.672	1
Vertical, upward	0.702	−1.219	−0.201	1

Note: experimental range
- 83,400<Re<163,000
- 30<Fr<61
- ρ_s/ρ_g=89 (O.P.=12.3 bar) & 133 (O.P.=7.8 bar)
- 0.4<μ_m<7.8

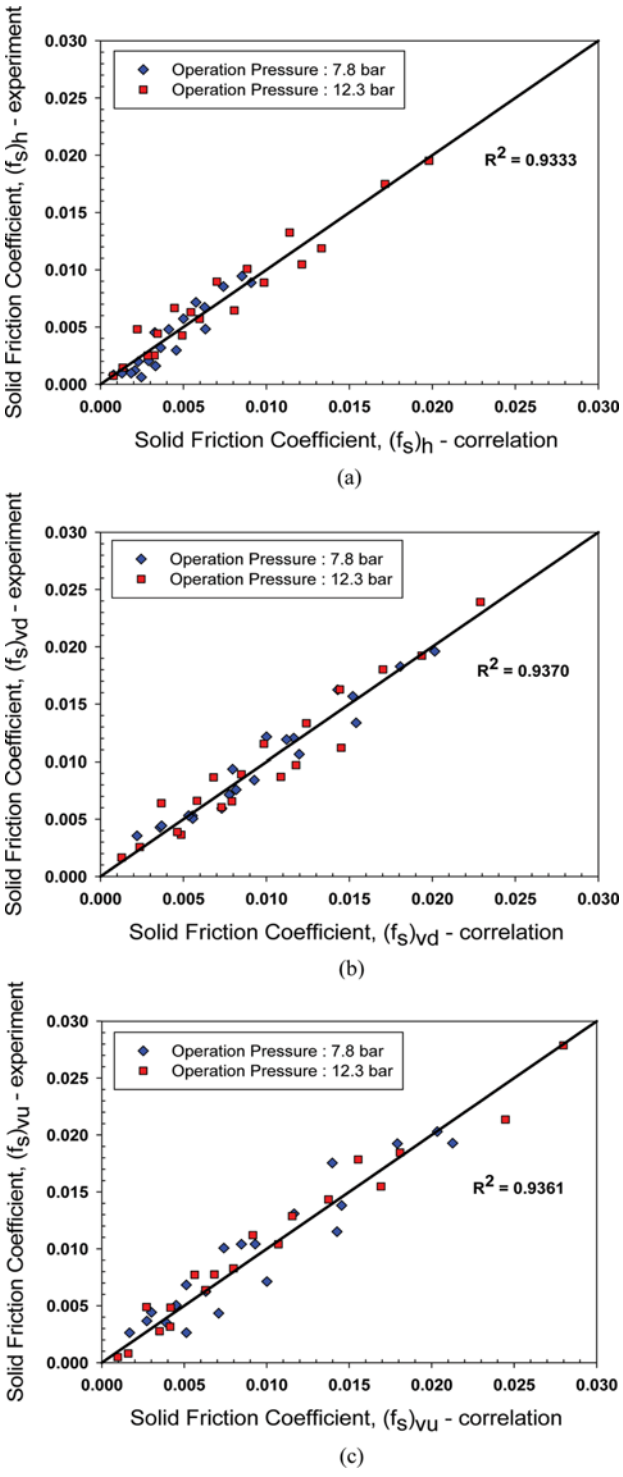

Fig. 7. The comparison between experimental results and relational expression of solid friction coefficients, for (a) horizontal, (b) vertical (downward), and (c) vertical (upward).

the correlation between relational expression and results of experiments were obtained. The exponents for each non-dimensional number in the expression (9) are summarized in Table 3. From Table 3, the impact of Froude number, which was the gravitational influence, appeared to be the most influential one in the vertical up-flow line, while the influence of density ratio was the most influential one in the horizontal line.

Relationships between results of experiments and correlation as represented in the expression (9) are illustrated in Fig. 7. For all cases of horizontal and vertical (both upward and downward) ones, the correlation between experimental results and derived relational expression was quite obvious, so the integrity of initial values obtained from the experiments was presumed to be sound.

Finally, the pressure loss coefficients at bend which would be configured into the transport line inevitably were derived. Pressure loss coefficients at the bend represented in expression (4) can be expressed in terms of gas and solid particle entrainment influences, and following correlation expression (10) was presented by prior study [21].

$$\Delta P = K\frac{1}{2}\rho_g v_g^2 = B(1+C\mu_m)\frac{1}{2}\rho_g v_g^2 \tag{10}$$

In the above expression (10), the B=0.5 and C=1.0 when R/D, the ratio of diameter of transport line (D) and radius of curvature of the tube (R), exceeds 6 [21]. And in this study, considering the quite big particle size which was not dealt with in prior studies, the rather generalized expression (11) than the expression (10) was employed to express the pressure loss coefficient.

$$K = K_g + K_s = K_g(\mathrm{Re}) + K_s\left(\mathrm{Fr}, \frac{\rho_s}{\rho_g}, \mu_m\right) \tag{11}$$

First, computational fluid dynamics (CFD) analyses for the pure gas flow field were conducted by applying the same diameter (D) and radius of curvature (R) of the line in the experiments of this study to examine the effect of gas and the variation of the Reynolds number Re. The range of Re used in this study was reflected, and the analysis for higher Re was separately conducted in view of the large scaled equipment and high operation pressure; the results thus obtained are illustrated in Fig. 8(a) and comprehensively described by the following expression (12):

$$K_g = K_g(\mathrm{Re}) = 5.554/\mathrm{Re}^{0.184} \tag{12}$$

When the Re was very high, the Re values tended to converge to the value of B=0.5, which was defined in the reference [21]. On the other hand, for lower Re range, the aforementioned B values were higher than 0.5. And then, the algebraic expression for the effect of solid particles in flow field on the pressure loss coefficient, the following functional expression (13) was introduced, combining non-dimensional numbers in the same way as the friction coefficient in the transport line.

$$K_s = K_s\left(\mathrm{Fr}, \frac{\rho_s}{\rho_g}, \mu_m\right) = A\mathrm{Fr}^{\alpha}\left(\frac{\rho_s}{\rho_g}\right)^{\beta}\mu_m^{\gamma} \tag{13}$$

The K_s was obtained by excluding K_g of the expression (12) from the K of (11), which obviously reflected the experimentally verified linearity relation with variation of solid loading ratio μ_m.

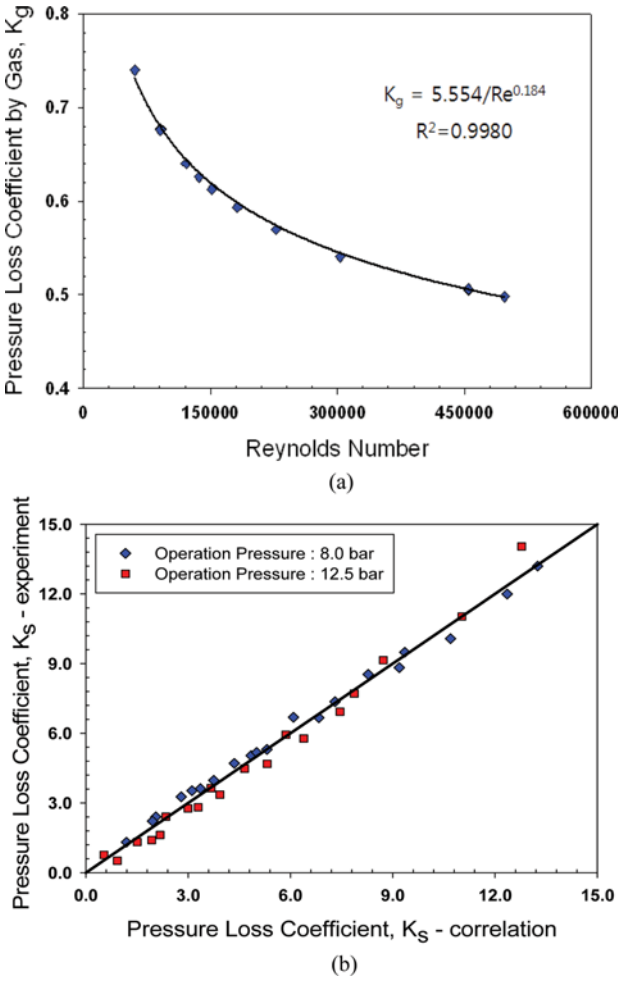

Fig. 8. (a) Pressure loss coefficients of pure gas flow at bend, and (b) comparison of outcomes from experiments and correlation expression.

The values of A=10.03, α=−0.788, and β=0.241 were correlated to maximize their effects on K_s by fixing the value of exponent for μ_m as 1. From this, the quite significant effect of Froude number on the pressure loss coefficient at bend was explained.

The functional relation thus obtained was experimentally substantiated as illustrated in Fig. 8(b). Such correlation also revealed reliability of the present experimental approach. Furthermore, following the method of the reference [21], the expression similar to (10) was introduced to reflect the effect of pressure loss coefficient and μ_m. Considering the relatively low domain of Re, the effect of pure gas was comprehensively reflected in the expression (14) instead of taking simple constant value.

$$K = K_g + K_s = K_g(\mathrm{Re})(1+C\mu_m) \tag{14}$$

The approximate value of C=2.5 was obtained using (12) for the K_g of pure gas flow field. The obtained value was quite larger than the value of C=1.0 expected from (10), following the method of reference [21]. This implies the significant dominance of K along with the increase of μ_m at each bend in view of the increase of integrated friction coefficient by 2-3 times compared with the case of pure gas transportation under relatively higher μ_m in horizontal

and vertical transport lines. In the bend, particles tend to concentrate on the concave part of outer part of pipeline by the centrifugal force created by gas flow and rapid increase in local number density and subsequent agglomeration of particles could occur. The pressure loss of transport gas thus increased significantly. The value of C=1.0 would be appropriate when particle sizes were small and the μ_m is low, following reference [21]. However, the pressure loss caused by the solid particles was significant, considering flow field of relatively high μ_m and larger particle size. This is attributed to the number of bends which should be minimized for transport of the particles with larger diameter at high μ_m. Thus it warrants further studies employing additional numerical analyses and/or experiments.

In view of the 'similitude and dimensional analysis' approach used in the present study, the aforementioned results should be valid for the wide range of diameters and lengths of smooth tubes, although the experimental results were obtained for a constant diameter tube. However, the present results might not be applicable for the transport pipe of higher wall roughness.

CONCLUSIONS

The mass flow rate and the solid loading ratio of the pulverized coal along with varied operation parameters were observed in the pneumatic transport equipment which fluidizes the pulverized coal in the pressurized vessel and discharges them upward. In the experiments conducted with the pulverized coal having very big particle diameters, the most influential factor upon mass flow rate of pulverized coal and solid loading ratio was the differential pressure between injection hopper and receive tank. Effect of the fluidization nitrogen flow rate on the present system was found to be a very important factor. And as a result, a similar mass flow rate of pulverized coal and solid loading ratio was obtained by increasing the differential pressure with equal amount of fluidization nitrogen supply in case when the transport line was extended.

The friction coefficient expressing the pressure drop in straight line and the pressure loss coefficient at each bend were represented by separate terms of gas flow influences and entrained solid particles to be expressed as a function of several non-dimensional numbers. The relational expression represented by non-dimensional numbers revealed quite high correlation with results of experiments, and from this, the integrity of raw data obtained from experimental results was identified to be sound enough. The exponents of non-dimensional numbers in relational expressions obtained from straight line were compared with each other, and the gravitational influence upon vertical up-flow line was identified to have the strongest impact compared to those of vertical down-flow or horizontal transport line. It was also observed that the pressure loss coefficient at bend tended to increase rapidly in accordance with the increase of solid loading ratio.

ACKNOWLEDGEMENTS

This work was supported by the Energy Efficiency & Resources program of the Korea Institute of Energy Technology Evaluation and Planning (KETEP) grant funded by the Korea government Ministry of Knowledge Economy (No. 2011T100200037).

REFERENCES

1. C. Higman and M. Burgt, Gasification, 2nd Ed., Gulf Professional Publishing (2008).
2. J. Volk, *Shell coal gasification: Delivering performance in Chinese operations*, Gasification Technology Conference, Washington D.C., U.S.A. (2010).
3. K. Radtke, *Global update on PRENFLO and HTW gasification technologies and applications*, Gasification Technology Conference, Washington D.C., U.S.A. (2012).
4. J. Crew, *GE gasification project update*, Gasification Technology Conference, Washington D.C., U.S.A. (2012).
5. P. Amick, *E-Gas technology 2012 outlook*, Gasification Technology Conference, Washington D.C., U.S.A. (2012).
6. J. Lee, S. Chung, S. Lee, W. Jung, Y. Byun, S. Hwang, D. Jeon, S. Ryu, J. Lee, K. Jeong, J. Kim and Y. Yun, *Korean Chem. Eng. Res.*, **52**(5), 657 (2014).
7. H. Ra, M. Seo, S. J. Yoon, S. M. Yoon, J. Kim, J. Lee and S. Park, *Korean J. Chem. Eng.*, **31**(9), 1570 (2014).
8. S. Ariyapadi, *TRIG™ technology - Applications for IGCC, refueling, and syngas projects*, Gasification Technology Conference, Washington D.C., U.S.A. (2012).
9. L. Lee, T. Quek, R. Deng, M. Raya and C. Wang, *Chem. Eng. Sci.*, **59**, 4637 (2004).
10. S. Mallick, *Modeling of fluidised dense-phase pneumatic conveying of powders*, Ph. D. thesis, University of Wollongong, Australia (2009).
11. J. Hilton and P. Cleary, *The role of particle shape in pneumatic conveying*, Seventh International Conference on CFD in the Minerals and Process Industries, Melbourne, Australia (2009).
12. L. Dhole, L. Bhuyar and G. Awari, *VSRD Int. J. of Mechanical, Automobile & Production Engineering*, **1**(1), 19 (2011).
13. C. Ratnayake, *Scaling up technique for pneumatic transport systems*, Ph. D. thesis, Telemark University College, Norway (2005).
14. D. Mills, *Pneumatic conveying design guide*, 2nd Ed., Elsevier Butterworth-Heinemann, Gulf Professional Publishing (2004).
15. S. Yoo., J. Lee, S. Chung, S. Yoon, J. Lee, M. Yi and S. Lim, *J. Energy & Climate Change*, **8**(1), 45 (by Korean) (2013).
16. R. Holdich, *Fundamentals of particle technology*, Midland Information Technology and Publishing (2002).
17. Y. Jo and M. Ray, *J. Ind. Eng. Chem. (Amsterdam, Neth.)*, **5**(1), 32 (1999).
18. C. Lee, J. Lee, G. Kim and J. Shin, *Computational analyses on coal-conveying pneumatic system*, 23rd International Society of Offshore and Polar Engineering, Anchorage, U.S.A. (2013).
19. C. Lee, J. Lee, G. Kim and T. Kwon, *Numerical simulations and correlations on the coal-conveying gas flow in pipe for fluidized-bed coal gasification facility*, Ecology and Safety 2014, 23rd International Conference, Elenite, Bulgaria (2014).
20. C. He, X. Chen, J. Wang, H. Ni, Y. Xu and H. Zhou, *Powder Technol.*, **227**, 51 (2012).
21. Pneumatic handling of powdered materials, The Engineering Equipment Users Association (EEUA) Handbook, No. 15, Constable and Company Ltd. (1963), quoted in S. Dhodapkar, P. Solt, K. Klinzing, Understanding bends in pneumatic conveying systems, Chemical Engineering (www.che.com), April , 53 (2009).